OPEN ACCESS Freely available online PLoS PATHOGENS

Listeria monocytogenes Invades the Epithelial Junctions at Sites of Cell Extrusion

Mickey Pentecost[1], Glen Otto[2], Julie A. Theriot[1,3☯], Manuel R. Amieva[1,4☯*]

1 Department of Microbiology and Immunology, Stanford University, Stanford, California, United States of America, **2** Department of Comparative Medicine, Stanford University, Stanford, California, United States of America, **3** Department of Biochemistry, Stanford University, Stanford, California, United States of America, **4** Department of Pediatrics, Stanford University, Stanford, California, United States of America

Listeria monocytogenes **causes invasive disease by crossing the intestinal epithelial barrier. This process depends on the interaction between the bacterial surface protein Internalin A and the host protein E-cadherin, located below the epithelial tight junctions at the lateral cell-to-cell contacts. We used polarized MDCK cells as a model epithelium to determine how *L. monocytogenes* breaches the tight junctions to gain access to this basolateral receptor protein. We determined that *L. monocytogenes* does not actively disrupt the tight junctions, but finds E-cadherin at a morphologically distinct subset of intercellular junctions. We identified these sites as naturally occurring regions where single senescent cells are expelled and detached from the epithelium by extrusion. The surrounding cells reorganize to form a multicellular junction that maintains epithelial continuity. We found that E-cadherin is transiently exposed to the lumenal surface at multicellular junctions during and after cell extrusion, and that *L. monocytogenes* takes advantage of junctional remodeling to adhere to and subsequently invade the epithelium. In intact epithelial monolayers, an anti-E-cadherin antibody specifically decorates multicellular junctions and blocks *L. monocytogenes* adhesion. Furthermore, an *L. monocytogenes* mutant in the Internalin A gene is completely deficient in attachment to the epithelial apical surface and is unable to invade. We hypothesized that *L. monocytogenes* utilizes analogous extrusion sites for epithelial invasion in vivo. By infecting rabbit ileal loops, we found that the junctions at the cell extrusion zone of villus tips are the specific target for *L. monocytogenes* adhesion and invasion. Thus, *L. monocytogenes* exploits the dynamic nature of epithelial renewal and junctional remodeling to breach the intestinal barrier.**

Citation: Pentecost M, Otto G, Theriot JA, Amieva MR (2006) *Listeria monocytogenes* invades the epithelial junctions at sites of cell extrusion. PLoS Pathog 2(1): e3.

Introduction

Listeria monocytogenes, a Gram-positive, facultative intracellular bacterial pathogen, is a source of human foodborne illness [1,2]. It was first discovered as a causative agent of septicemia in rabbits [3]. In humans it causes a range of clinical manifestations from asymptomatic intestinal carriage and gastroenteritis to invasive and disseminated disease. Septicemia, meningoencephalitis, and infection of the fetus in pregnant women are the most serious manifestations of listeriosis [1]. The gastrointestinal tract is the primary site of entry for pathogenic *Listeria* species, and contaminated food is the major source of infection in both epidemic and sporadic cases [4,5]. After invasion of the small intestine, *L. monocytogenes* can spread to and infect the liver, spleen, central nervous system, and, in pregnant women, the placenta [1].

Invasion of non-phagocytic cells by *L. monocytogenes* is mediated by at least two bacterial surface proteins, Internalin A (InlA) and Internalin B (InlB) [6–8]. InlA binds an extracellular domain of E-cadherin, a transmembrane cell-to-cell adhesion molecule [9–13]. InlA is necessary for invasion of epithelial cells and is sufficient to reconstitute invasion when expressed in the non-pathogenic and non-invasive species, *Listeria innocua* [6,9,11]. InlB binds the extracellular domain of c-Met, a receptor tyrosine kinase [14]. Although InlB is unrelated by sequence or structure to the endogenous c-Met ligand, hepatocyte growth factor, it acts as an exogenous c-Met agonist and mediates *L. monocytogenes* invasion of multiple cell types [8,14–23]. InlB acts synergistically with InlA during invasion of cultured epithelial cells through an unknown mechanism [8,17,24].

The anatomical site and the mechanism by which *L. monocytogenes* breaches the intestinal epithelial barrier are controversial. In mice, *L. monocytogenes* invasion and replication within the gastrointestinal tract is independent of InlA and is restricted to the Peyer's patches, suggesting a predominant role for specialized phagocytic M-cells in bacterial uptake [13,25–28]. Similarly in rats, intestinal translocation rates are low and independent of the *inlAB* locus, suggesting a passive process that does not involve InlA or InlB [29]. However, mice and rats are not natural hosts for *L. monocytogenes*. Furthermore, mouse and rat E-cadherin differ from human E-cadherin at an important amino acid residue that renders cells resistant to InlA-mediated invasion [13]. In contrast, *L. monocytogenes* can directly invade enterocytes in guinea pigs, which are naturally susceptible to listeriosis [27,30]. In transgenic mice, enterocytes expressing human E-cadherin are also susceptible to invasion by *L. monocytogenes* [27].

Editor: Pascale Cossart, Institut Pasteur, France

Received October 18, 2005; **Accepted** December 19, 2005; **Published** January 27, 2006

DOI: 10.1371/journal.ppat.0020003

Abbreviations: CFU, colony forming unit; GFP, green fluorescent protein; IM, intramuscular; InlA, Internalin A; InlB, Internalin B; MDCK, Madin-Darby canine kidney; MOI, multiplicity of infection; PBS, phosphate-buffered saline; Wt, wild-type

* To whom correspondence should be addressed. E-mail: amieva@stanford.edu

☯ These authors contributed equally to this work.

Synopsis

Studies in microbial pathogenesis are just beginning to address how epithelial cell polarity and host tissue architecture influence host-pathogen interactions. It has long been known that *Listeria monocytogenes* invasion of epithelial cells requires binding of host cell E-cadherin, a cell-to-cell junction protein. However, an ongoing question has been how *L. monocytogenes* reaches this receptor, since E-cadherin is located in the basolateral membrane of enterocytes and is inaccessible to bacteria in the intestinal lumen. By examining polarized epithelial monolayers in tissue culture and rabbit intestine in vivo, the authors investigate how and where *L. monocytogenes* breaches the tight junctions to interact with E-cadherin and invade. They show that *L. monocytogenes* takes advantage of a temporal window of junctional reorganization that exposes E-cadherin at sites where senescent cells are extruded and removed from the epithelium. In the small intestine, cell extrusion is confined to the tips of the intestinal villi, and the authors show that junctions at the villus tips are the sites of *L. monocytogenes* invasion in vivo. If basolateral proteins are exposed at cell extrusion sites, do other microbes that utilize basolateral cellular receptors also find them?

How *L. monocytogenes* gains access to E-cadherin in vivo remains an important and unresolved issue, since E-cadherin is present primarily on the lateral membranes, but not on the apical surface, of intestinal epithelial cells [31–33]. Several lines of evidence suggest that *L. monocytogenes* invade polarized epithelial cells most efficiently from the basolateral side [34,35]. First, *L. monocytogenes* preferentially infect the lateral edges of islets of cultured epithelial cells [34,35]. Second, *L. monocytogenes* invasion decreases with epithelial monolayer maturity. Third, *L. monocytogenes* invasion of a confluent epithelial monolayer can be increased by disrupting the intercellular junctions, thereby exposing lateral cell membranes [34]. It has been proposed that *L. monocytogenes* gain access to E-cadherin during an apical infection through the activation of c-Met by InlB [36]. However, c-Met is also a basolateral receptor and is not known to be exposed or activated by hepatocyte growth factor on the apical side of epithelia [37,38].

We used Madin-Darby canine kidney (MDCK) cells to investigate how *L. monocytogenes* breaches the apical surface of an epithelial barrier. We chose this cell line because MDCK cells form a polarized epithelium with tight junctions when grown on permeable filter supports [39], and because MDCK cells are permissive for *L. monocytogenes* invasion [40]. Moreover, canine E-cadherin is identical to human E-cadherin in the critical InlA binding region, and InlB activates c-Met signaling in MDCK cells [14]. We show here that apical invasion of an MDCK epithelium by *L. monocytogenes* regularly occurs and is critically dependent on the interaction between InlA and E-cadherin. Detailed microscopic analyses of adhesion and entry reveal that *L. monocytogenes* has a specific tropism for the junctions at cell extrusion sites where E-cadherin is transiently exposed to the apical surface. This mode of entry suggested that *L. monocytogenes* invasion and translocation of the small intestine might occur at the apical tips of the intestinal villi, where enterocytes apoptose and are expelled into the intestinal lumen by a normal mechanism of cell extrusion. We confirmed this hypothesis in a rabbit ileal loop infection model [41].

Results

L. monocytogenes Invades the Epithelium at Distinct Multicellular Junction Sites

We infected polarized MDCK monolayers on Transwell filters from the apical or basal side to determine whether *L. monocytogenes* differentially invade these two membrane domains. After 10 min, the monolayers were washed to remove non-adherent bacteria, and the cell-associated *L. monocytogenes* were allowed to invade the epithelium for 1 h. Any remaining extracellular bacteria were killed with gentamicin for 20 min, and viable intracellular *L. monocytogenes* were quantified. Bacterial infection in these conditions did not disrupt the integrity of the monolayer (Figure S1). Basal invasion of a polarized MDCK epithelium is 5-fold more efficient than apical invasion (Figure 1A), despite the fact that the filter support masks 85% of the basal surface area. We tested a range of multiplicity of infections (MOIs) from 1 to 150 bacteria per cell and found that the higher level of basal invasion is independent of the infectious dose ($p < 0.01$). However, at all inocula tested, there was a detectable level of apical invasion.

We analyzed the sites of apical versus basal invasion by confocal immunofluorescence microscopy. At various time points after internalization, monolayers were fixed and probed with antibodies to *L. monocytogenes*. The infected monolayers were counterstained for the tight junctions (anti–ZO-1). We observed that sites of basal infection were distributed throughout the monolayer (Figure 1B). In contrast, we noted that after apical infection, *L. monocytogenes* concentrate at distinct sites where multiple (five or more) elongated cells join at a central multicellular junction (Figure 1C–1F). By 3 h of infection, small foci of replicating bacteria are found within cells at multicellular junction sites (Figure 1D), and by 5 h, large foci of bacteria are localized at the original sites of entry (Figure 1E). These bacteria were viable and replicative, since they had acquired actin-based intracellular motility as indicated by the associated tail of polymerized actin (Figure 1D, inset) [40,42–44]. Virtually all *L. monocytogenes* foci (97% ± 1.1%, mean ± SD; 3 h post-infection) are centered at multicellular junctions made by five or more MDCK cells. However, multicellular junctions are specialized sites of invasion only from the apical side. In contrast to apical infection, less than 1% of basally infected cells were associated with a multicellular junction joining five or more cells (Figure 1B).

To confirm that cells with multicellular junctions are the primary sites of apical invasion, we used a mutant of *L. monocytogenes* that invades host cells normally but is unable to spread to adjacent cells because it lacks the *actA* gene, which is necessary for actin-based cell-to-cell spread (Δ*actA*, Figure 1F) [43,45]. At 3 h post-infection, Δ*actA L. monocytogenes* infected cells are members of multicellular junction sites with a frequency of 97% ± 0.8%.

Apical Attachment to Multicellular Junctions Is Dependent on Internalin A

We infected polarized MDCK monolayers with wild-type (Wt) *L. monocytogenes*, an *inlA*-deletion mutant (Δ*inlA*), or an *inlB*-deletion mutant (Δ*inlB*) to determine which invasins are needed for apical invasion. Following a period of internalization, the infected monolayers were treated with gentami-

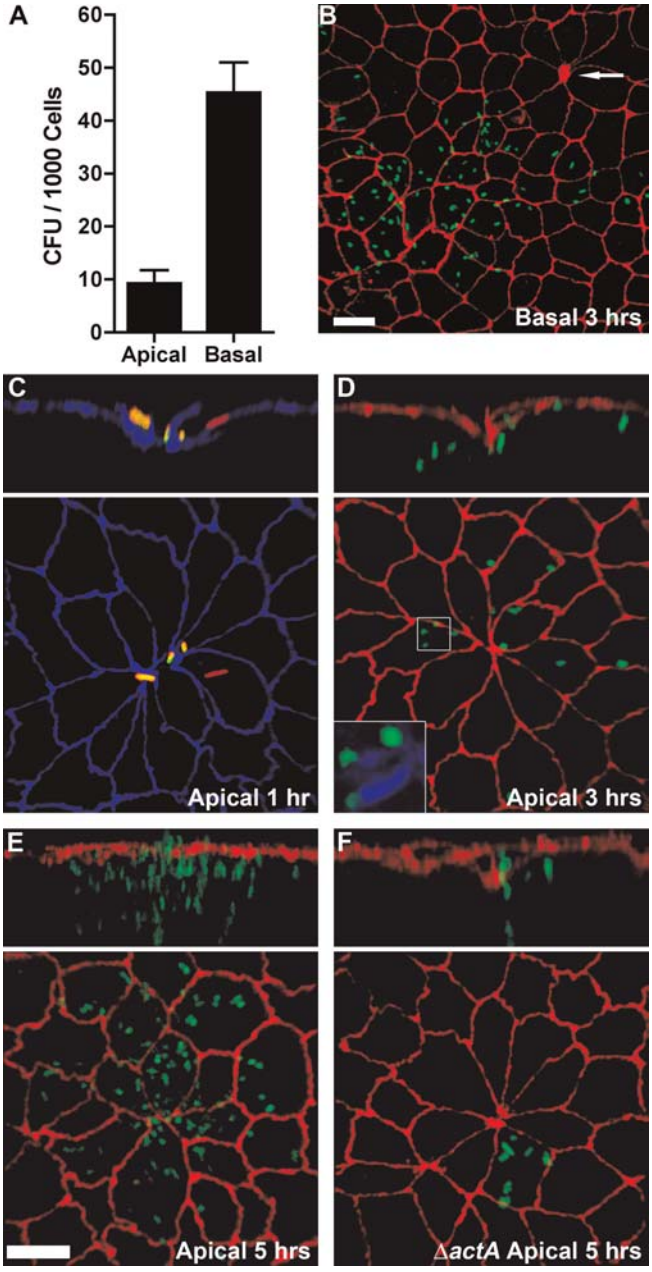

Figure 1. Invasion and Replication of *L. monocytogenes* at Multicellular Junction Sites

Polarized MDCK monolayers on Transwell filters were infected from the apical (A, C–F) or basal (A and B) sides with *L. monocytogenes*.
(A) Viable CFUs of intracellular *L. monocytogenes* were determined after gentamicin treatment. Means and standard deviations from quadruplicate samples are shown. Sample groups are significantly different: unpaired *t*-test $p < 0.0001$.
(B–D) Three-dimensional reconstructions of confocal immunofluorescence images of the invasion sites. Upper panels are reconstructions of Z-sections.
(B) At 3 h after basal infection, foci of replication were visualized with antibodies to *L. monocytogenes* (green) and ZO-1 (red). Arrow indicates a multicellular junction site.
(C) At 1 h after apical infection, a representative site of invasion was visualized with antibodies to ZO-1 (blue). To evaluate intracellular versus extracellular bacteria, we performed an inside/outside staining where extracellular adherent *L. monocytogenes* were stained before permeabilization in green and both intracellular and extracellular bacteria were stained after permeabilization in red. External *L. monocytogenes* thus appear as a combination of red/green or yellow.
(D) At 3 h after apical infection, sites of replication were visualized with antibodies to *L. monocytogenes* (green) and ZO-1 (red), and with phalloidin (blue) to show actin comet-tails in association with the cytoplasmic bacteria, inset.
(E) At 5 h after apical infection, foci of replication and spread were visualized with antibodies to ZO-1 (red) and *L. monocytogenes* (green).
(F) Using the same methodology as in (E), monolayers were infected with Δ*actA L. monocytogenes* (green), which are capable of cell invasion and intracellular replication but not cell-to-cell spread.
Scale bars 10 μm.
DOI: 10.1371/journal.ppat.0020003.g001

cin and then the number of viable intracellular bacteria was determined (Figure 2). Apical invasion requires InlA, since Δ*inlA L. monocytogenes* invasion is almost eliminated (2% of Wt, Figure 2A). Invasion by Δ*inlB L. monocytogenes* is also reduced (43% of Wt, Figure 2A). However, when Δ*inlB* invasion was analyzed by confocal microscopy, the tropism for multicellular junction sites remained (98% ± 1.4% of foci; 3 h post-infection).

To determine whether the defects in invasion are due to defects in attachment, we infected polarized MDCK monolayers for 10 min, removed non-adherent bacteria, and quantified attachment by confocal immunofluorescence

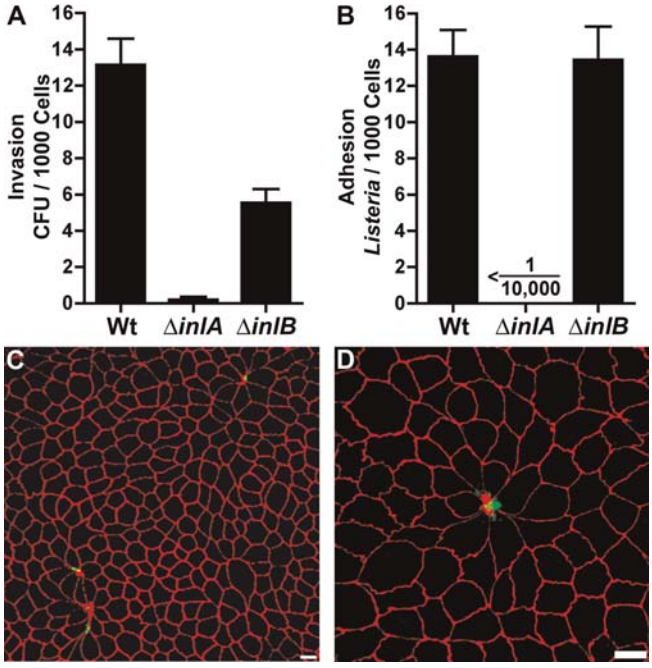

Figure 2. Internalin A–Dependent Apical Adhesion and Invasion of Polarized Epithelia

(A and B) Polarized MDCK monolayers were infected from the apical side with Wt, Δ*inlA,* or Δ*inlB L. monocytogenes*.
(A) Invasion was determined by quantification of viable CFUs of intracellular bacteria after gentamicin treatment. Means and standard deviations from quadruplicate samples are shown. Sample groups are significantly different: one-way analysis of variance $p < 0.0001$; Bonferroni *t*- test $p < 0.001$ for all pairwise analyses.
(B) Adhesion after 10 min of infection. Means and standard deviations of the number of *L. monocytogenes* adhered per 1,000 cells from triplicate samples are shown.
(C) Confocal microscopy visualization of Wt *L. monocytogenes* adhered to a monolayer stained with antibodies to *L. monocytogenes* (green) and ZO-1 (red). Bacteria are found only at multicellular junctions and are conspicuously absent elsewhere.
(D) A higher magnification area demonstrating concentrated adhesion at a multicellular junction. Scale bars 10 μm.
DOI: 10.1371/journal.ppat.0020003.g002

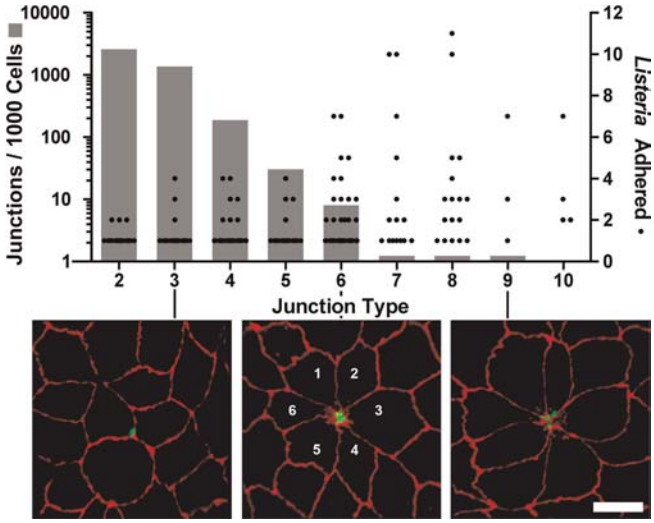

Figure 3. Tropism of *L. monocytogenes* for Multicellular Junctions

Cell junction types and *L. monocytogenes* adhesion sites were analyzed by quantitative confocal microscopy. The grey bars (left, *y*-axis) represent the frequency of junction types, defined as the number of cells that meet at a junction, based on analysis of three randomly imaged regions (~500 cells/region) of a polarized MDCK monolayer. The black circles (right, *y*-axis) represent the number of *L. monocytogenes* adhered per junction type. Pearson correlation coefficient $r = 0.95$, $p = 0.0001$. Bottom: examples of adhesion sites shown by confocal microscopy and visualized with antibodies to *L. monocytogenes* (green) and ZO-1 (red). *L. monocytogenes* adhered to multicellular junctions with 3, 6, and 9 cells are shown. Scale bar 10 μm.

DOI: 10.1371/journal.ppat.0020003.g003

microscopy. The vast majority of Wt *L. monocytogenes* (98% ± 1.5%) attach to polarized MDCK monolayers directly above ZO-1 staining, the site of the tight junctions (Figure 2C, 2D), and adhesion, like invasion, is concentrated at multicellular junction sites (Figure 2C, 2D). Adhesion is entirely dependent on InlA, since we did not find any Δ*inlA L. monocytogenes* associated with the epithelium using an equivalent inoculum (Figure 2B). In contrast, Δ*inlB L. monocytogenes* adheres to polarized MDCK monolayers as frequently (Figure 2B) and as specifically to the junctions (98% ± 1.2%) as Wt. These results suggest that InlA is the major adhesin, that adhesion is required for entry, and that InlB contributes to internalization but not attachment.

Quantitative Analysis of *L. monocytogenes* Adhesion Sites

To quantitatively define the tropism between *L. monocytogenes* and multicellular junctions, we first characterized the frequency and distribution of multicellular junctions throughout the monolayer, and then related this to sites of bacterial attachment. Each cell in an epithelium joins more than one cell through a cell-to-cell junction. However, a fraction of cell junctions joins a group of cells at a single point to form a multicellular junction. The number of cells that come together to form a junction can be used to define a "junction type." In Figure 3 we plotted the frequency of each junction type in the form of a bar graph, noting that junction types with increasing multicellularity are less common. To determine whether there is a preferred junction type for *L. monocytogenes* adhesion, we counted the number of *L. monocytogenes* associated with each junction type, and plotted these, too, in Figure 3. We find an increasing number of bacteria colocalize with junctions joining an increasing number of cells (Figure 3, Pearson correlation coefficient for Wt *L. monocytogenes* $r = 0.95$, $p = 0.0001$; Δ*inlB L. monocytogenes* $r = 0.85$, $p = 0.0037$). This correlation between increasing multicellularity at a junction and bacterial attachment is striking, given that the frequency of multicellular junctions rapidly decreases. Overall, 74% of *L. monocytogenes* were adhered at multicellular junctions joining five or more cells, which represent only 2% of all junctions.

We found no indication that *L. monocytogenes* induce these sites through alterations of cellular or junctional morphology, since infected and uninfected monolayers have the same frequencies of junctional types, and since *L. monocytogenes* are associated with these sites rapidly, within 5 to 10 min of infection. We therefore concluded that *L. monocytogenes* take advantage of preexisting multicellular junctions as a special site on the epithelial surface that permits adhesion and invasion.

Multicellular Junctions Form and Persist at Sites of Cell Extrusion

Since junctions are dynamic structures, we asked when and where multicellular junctions form in an MDCK epithelium. Sites with similar morphology were shown to develop when apoptotic cells are extruded from the epithelial monolayer into the apical media [46,47]. We confirmed that multicellular junctions form during cell extrusion in uninfected MDCK monolayers and analyzed the kinetics of this process by time-lapse video microscopy (Figure 4A, Video S1). A cell targeted for extrusion is initially morphologically indistinguishable from the surrounding cells (Figure 4A, 0 h). Once the extrusion process is initiated, it occurs rapidly, within approximately 40 min (Figure 4A, 1 h), leaving a characteristic rosette-like arrangement of the surrounding cells with a central multicellular junction. This pattern of cellular and junctional organization is maintained for several hours longer than the actual extrusion event (Figure 4A, 6 h). No monolayer defects were detected at these sites, since the adjacent cells reorganize to maintain epithelial continuity.

To examine entire monolayers for sites of cell extrusion, we stained extruding cells with Sytox green and examined them by confocal immunofluorescence microscopy. This high affinity nucleic acid dye stains the nuclei of dying or dead cells but cannot cross the impermeable membranes of live cells. Sytox staining revealed cells in various stages of the extrusion process. Before a dying cell is extruded, the tight junctions surrounding the cell dip toward the basal side of the monolayer (Figure 4B–4D). When a cell is nearly extruded from the monolayer, the surrounding cells form a funnel-shaped multicellular junction below the plane of the Sytox-positive cell nucleus (Figure 4C). Even after the loss of Sytox-positive cells, staining of the epithelial monolayer nuclei can pinpoint extrusion sites since there is always a conspicuously missing nucleus at multicellular junctions joining five or more cells. Furthermore, the funnel-like rearrangement of junctions persists after extrusion has completed (Figure 4D).

L. monocytogenes Attachment Sites Are Sites of Cell Extrusion

To determine whether *L. monocytogenes* sites of adhesion are equivalent to sites of cell extrusion, we reexamined bacterial adhesion sites with regard to 1) the presence of extruding cells (Sytox), 2) missing nuclei (toto-3), and 3) the funnel-like

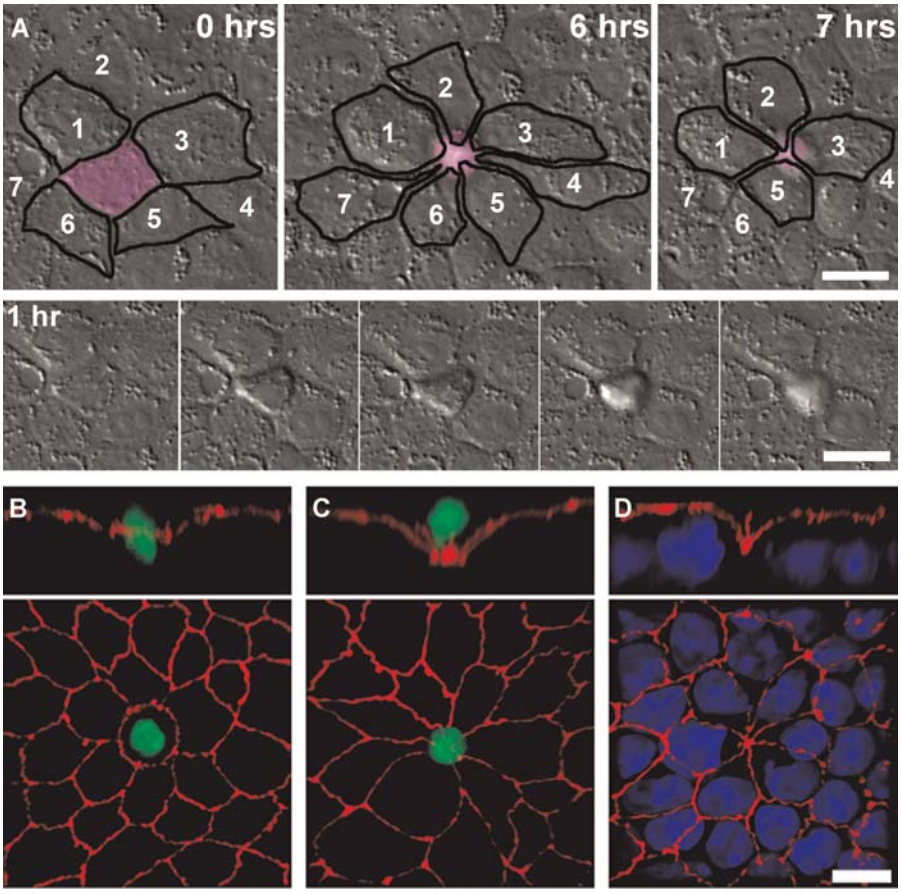

Figure 4. Multicellular Junctions Created by Cell Extrusion

(A) Top panels show reorganization of cells around a site of cell extrusion monitored live by time-lapse differential interference contrast microscopy. The extruding cell is colored in purple, and adjacent cells are outlined in black to show changes in the shape and relative location of the cells over time. The cells surrounding the extruded cell are numbered to illustrate their position at the start and after resolution of the multicellular junction. The bottom strip shows the process of extrusion, beginning at hour 1 of observation, and continuing for 40 min; frames at 10-min intervals.

Early (B) and late stages (C) of cell extrusion from a polarized MDCK epithelium were imaged by confocal microscopy after staining the monolayer for apoptotic nuclei with Sytox green and with antibodies to ZO-1 (red).

(D) Staining of all the cell nuclei in the monolayer with toto-3 (blue) illustrates that a missing nucleus is evident at extrusion sites after cell extrusion is completed. Reconstructed Z-section panels (B–D, top) reveal the rearrangement of junctions that occurs during cell extrusion.

Scale bar 10 μm.

DOI: 10.1371/journal.ppat.0020003.g004

rearrangement of the tight junctions (anti–ZO-1). Figure 5A shows that *L. monocytogenes* adheres to the junctions at sites where cells are in the process of extrusion (also see Video S2). These sites represent a small subset of multicellular junctions since the extrusion process occurs rapidly. All *L. monocytogenes* adhesion sites at multicellular junctions joining five or more cells have the characteristic absence of a nucleus (Figure 5B) and funnel-like rearrangement of the tight junctions (Figure 5A). Therefore, these are also sites where cell extrusion has occurred recently.

L. monocytogenes Adheres to Transiently Exposed E-cadherin at Sites of Cell Extrusion

We hypothesized that the molecular basis of apical adhesion might be E-cadherin exposed at cell extrusion sites, since Δ*inlA L. monocytogenes* do not adhere to the apical surface of polarized MDCK monolayers, whereas Wt and Δ*inlB L. monocytogenes* adhere primarily at multicellular junctions. Non-permeabilized polarized MDCK monolayers were incubated on the apical side with a monoclonal antibody that detects the extracellular domain of E-cadherin [48,49]. Apical E-cadherin is readily detected at the multicellular junctions associated with cells in the process of extrusion (Figure 6A) as well as at multicellular junction sites where an extruded cell has already been lost (Figure 6B). Adhered *L. monocytogenes* are commonly found over regions of apical E-cadherin exposure at cell junctions (Figure 6C). Furthermore, incubating polarized MDCK monolayers in low calcium medium, which disrupts the intercellular junctions, increases *L. monocytogenes* adherence to the epithelium specifically at intercellular regions where E-cadherin is exposed (Figure S2).

To confirm that the receptor for *L. monocytogenes* at multicellular junctions is E-cadherin and not a novel InlA receptor, we blocked apical E-cadherin by pretreating live MDCK monolayers with the anti–E-cadherin antibody, or the equivalent amount of antibody for the apical glycoprotein gp135 as a control [50]. To ensure that equal amounts of anti–E-cadherin and anti-gp135 antibodies were used, we determined the relative antibody concentrations using a quantitative dot blot analysis of the antibody solutions (Figure 6D).

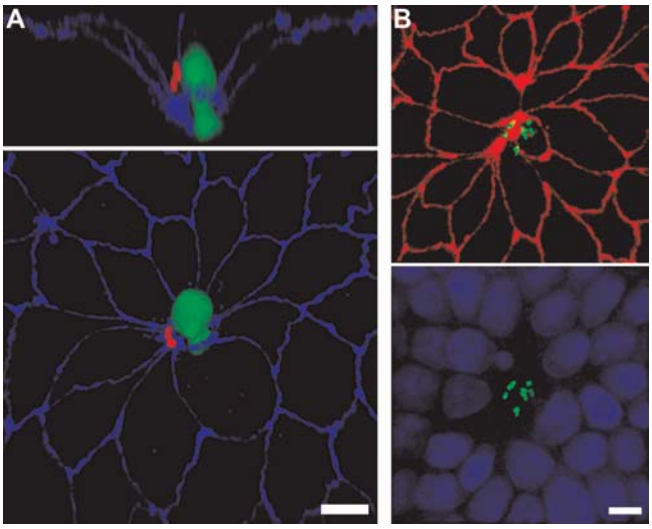

Figure 5. *L. monocytogenes* Adhesion to Sites of Cell Extrusion

Polarized MDCK monolayers on Transwell filters were infected from the apical side with Wt *L. monocytogenes* for 10 min.

(A) Extruding cells were stained with Sytox green prior to fixation. Antibodies to *L. monocytogenes* (red) were used to visualize adhered bacteria, and anti-ZO-1 (blue) antibodies were used to visualize the cell junctions.

(B) Monolayers were stained with antibodies to *L. monocytogenes* (green) and ZO-1 (red), and with toto-3 (blue), which illustrates missing nuclei at *L. monocytogenes* adhesion sites.

Scale bars 10 μm.

DOI: 10.1371/journal.ppat.0020003.g005

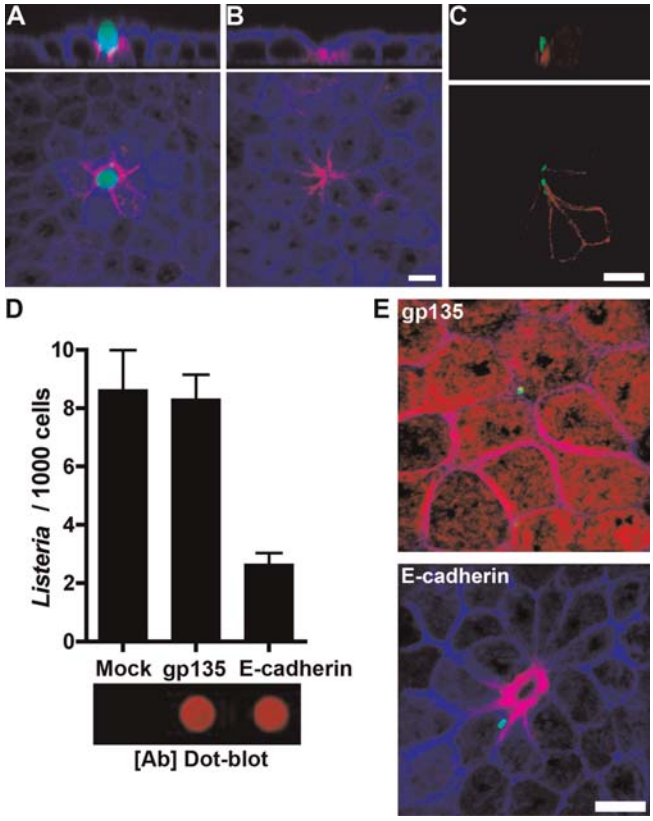

Figure 6. *L. monocytogenes* Attachment to Accessible E-cadherin at Multicellular Junctions of Cell Extrusion Sites

(A and B) Polarized MDCK monolayers on Transwell filters were incubated with Sytox green prior to fixation. Monolayers were left unpermeabilized and stained from the apical side with an antibody to the extracellular domain of E-cadherin (red) and with phalloidin to visualize the F-actin cytoskeleton (blue).

(A) A site with a cell in the process of extrusion.

(B) A site where extrusion has been completed.

(C) Polarized MDCK monolayers on Transwell filters were infected from the apical side with *L. monocytogenes* for 10 min, then stained from the apical side with antibodies to *L. monocytogenes* (green) and E-cadherin (red) without permeabilizing the sample.

(D) Polarized MDCK monolayers on Transwell filters were pretreated with anti-gp135 or anti–E-cadherin antibodies, then infected with *L. monocytogenes* for 5 min. Means and standard deviations of the number of *L. monocytogenes* adhered per 1,000 cells from triplicate samples are shown. The E-cadherin antibody–treated sample group is significantly different: one-way analysis of variance $p = 0.0004$. Bonferroni *t*-test Mock versus gp135 $p > 0.05$; Mock or gp135 versus E-cadherin $p < 0.001$. Shown below the bar graph, blocking antibody concentrations were normalized using a fluorescence-based dot-blot analysis ([Ab] Dot-blot).

(E) Confocal immunofluorescence images show the localization of the blocking antibodies (red), adhered *L. monocytogenes* (green) and the F-actin cytoskeleton (blue).

Scale bars 10 μm.

DOI: 10.1371/journal.ppat.0020003.g006

The anti-E-cadherin antibody, which only stains multicellular junctions, blocks adhesion by 70%. In contrast, the anti-gp135 antibody, which decorates the entire apical surface, has no effect on *L. monocytogenes* adhesion (Figure 6D and 6E). These results suggest that there exists a temporal window of junctional reorganization during cell extrusion that transiently exposes E-cadherin for adhesion of *L. monocytogenes*.

L. monocytogenes Invades Multicellular Junctions at the Villus Tip Extrusion Zone

In the small intestine, enterocytes are generated within the crypts and migrate up the lateral sides of the villi [51]. The apex of the villus is defined as the extrusion zone, where enterocytes undergo programmed cell death and are expelled into the intestinal lumen [51,52]. Therefore, in contrast to an MDCK epithelium, where cell extrusion occurs throughout the monolayer, cell turnover in vivo is temporally and spatially regulated.

Our cell culture results predicted that *L. monocytogenes'* invasion of intestinal epithelium would occur preferentially at the tips of the villi. We infected rabbit ileal loops with *L. monocytogenes* and examined the sites of in vivo attachment and entry to test this hypothesis. This experimental system was used because rabbits are natural hosts for *L. monocytogenes* and rabbits have InlA-permissive E-cadherin [3,13]. Figure 7 shows three-dimensional confocal reconstructions of villi from a rabbit ileal loop infected with 4×10^7 CFU/ml of Wt-GFP *L. monocytogenes* for 4 h. By imaging multiple 40× fields, we estimate that at least 50% of villi had *L. monocytogenes* associated with the villus tips (Figure 7B and Video S3). Although *L. monocytogenes* were embedded in the mucus above and between villi, we did not find *L. monocytogenes* associated with the epithelium along the lateral sides of the villi, or with cells of the intestinal crypts (Figures 7A and S2A). The same result was observed in ileal loops infected with Wt *L. monocytogenes* that do not express GFP visualized with anti–*L. monocytogenes* antibodies (unpublished data). We did not find *L. monocytogenes* associated with Peyer's patches (Figure S3), although there were *L. monocytogenes* associated with the tips of villi surrounding Peyer's patches (Figure S3C).

We determined that *L. monocytogenes* invasion preferentially occurs at the tips of the intestinal villi, since intracellular

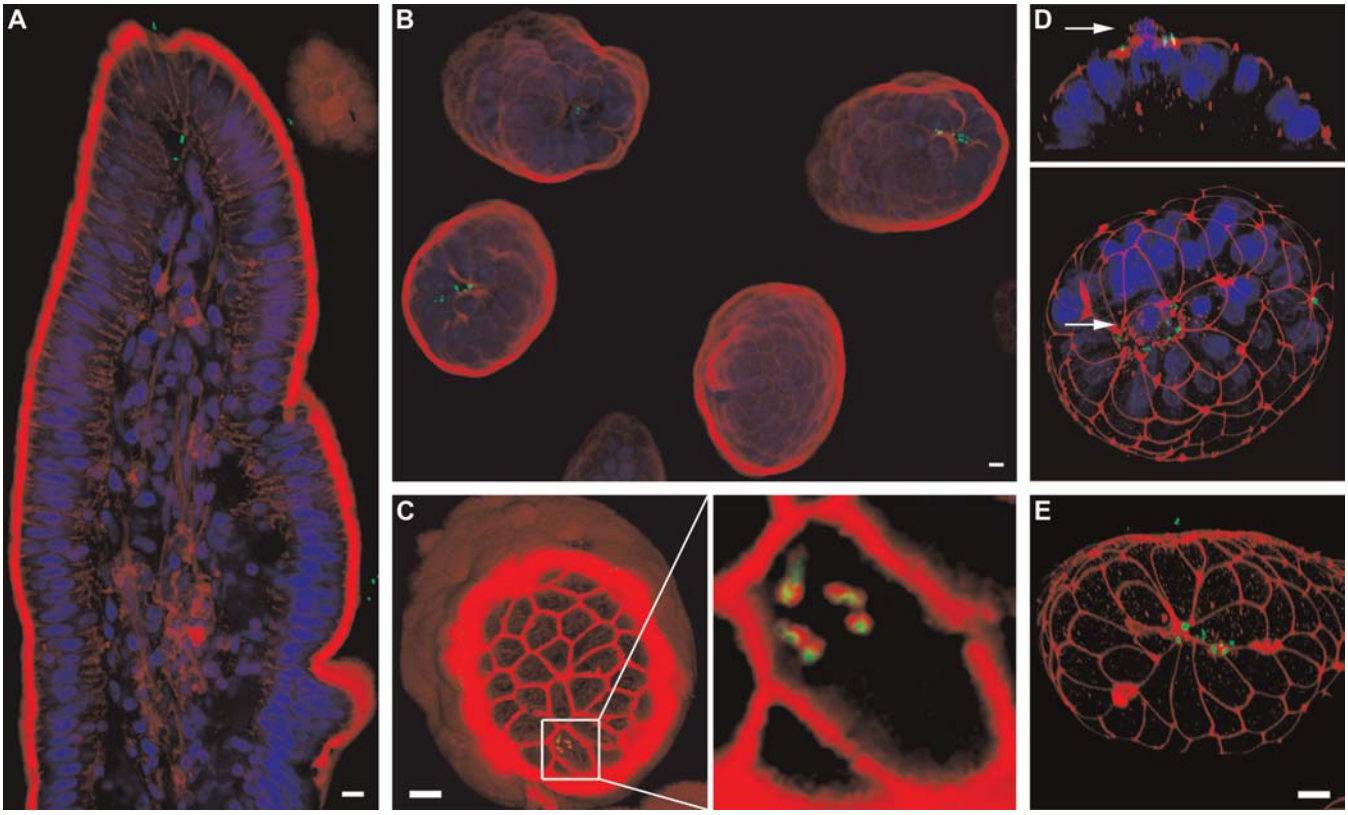

Figure 7. *L. monocytogenes* Invasion of the Intestinal Epithelium at the Villus-Tip Extrusion Zone

(A) Optical longitudinal section through a villus tip from Wt-GFP *L. monocytogenes* infected rabbit intestinal tissue stained with phalloidin for F-actin (red) and with toto-3 for nuclei (blue). GFP-expressing bacteria are shown in green.

(B) Three-dimensional reconstruction of villus tips viewed from the lumenal side from tissue stained as in (A).

(C) Optical cross-section through three-dimensional reconstruction of a villus tip revealing intracellular *L. monocytogenes* (green). F-actin (red) is stained with phalloidin. Right: enlarged view of infected cell revealing actin nucleation on the surface of Wt-GFP *L. monocytogenes*.

(D) Three-dimensional confocal reconstruction of villus tip from tissue stained with antibodies to ZO-1 (red) and with toto-3 for nuclei (blue). Arrow indicates a cell being extruded.

(E) Three-dimensional reconstruction of infected villus tip stained with antibodies to ZO-1 (red), showing a multicellular junction.

Scale bars 10 μm.

DOI: 10.1371/journal.ppat.0020003.g007

bacteria could only be found at the villus tips after the 4-h infection (Figure 7A). Some intracellular *L. monocytogenes* had already accumulated actin on their surfaces, indicating that they were viable and had escaped from the internalization vacuole (Figure 7C). As an additional control for the viability of internalized bacteria, we infected a rabbit ileal loop with a strain of *L. monocytogenes* carrying a transgene with monomeric red fluorescent protein fused to ActA (ActA-RFP) [53]. Since the ActA protein is expressed only after bacteria enter the host cell cytoplasm [54,55], these bacteria express ActA-RFP only after successful invasion [53]. ActA-RFP–expressing *L. monocytogenes* were only found at the tips of the villi (Figure S3D). Δ*inlA L. monocytogenes* at an inoculum of 4×10^8 CFU/ml failed to invade the epithelium (Figure S3E and Video S4).

We stained the infected intestinal tissues with anti–ZO-1 antibodies to determine whether in vivo adhesion and invasion of *L. monocytogenes* also occurs at multicellular junctions associated with extrusion. Adherent bacteria consistently colocalized with junctional staining, and were commonly found at multicellular junctions that occur in the extrusion zone of the villus tips (Figure 7E). Similar to our results in MDCK cell cultures, staining for nuclei of enterocytes in the villi revealed that *L. monocytogenes* readily associate with the junctions surrounding extruding cells (Figure 7D). These results indicate that the sites of apoptotic cell extrusion from an epithelium are uniquely permissive for *L. monocytogenes* invasion in vivo as well as in tissue culture.

Discussion

Many pathogenic microbes preferentially interact with constituents of basolateral epithelial cell membranes for invasion [33,56]. For example, the parasite *Toxoplasma gondii* somehow breaches the tight junctions to migrate between cells [57]. Rotaviruses bind integrins, a class of adhesion and signaling molecules found solely on the basolateral sides of enterocytes [58]. The bacterium *Shigella flexneri*, like *Listeria monocytogenes,* preferentially invades the basolateral membranes of polarized epithelial cells [34,59]. Paradoxically, the basolateral aspect of epithelial cells is not readily accessible to most microbes. In addition to the mechanical clearing mechanisms and immune defenses of the lumenal compartment, the tight junctions of epithelia restrict access to the basolateral membrane domain. Some pathogens have evolved mechanisms to undermine, modify, or bypass the epithelial tight junctions. For example, *Vibrio cholerae* secretes a protease

that can degrade the tight junction protein occludin [60]. *Helicobacter pylori* and enteropathogenic *E. coli* disrupt the junctions from the inside out by injecting effector proteins into epithelial cells [61,62]. Yersinia circumvent the tight junctions of enterocytes by accessing β1-integrin receptors exposed on the apical surface of M-cells [63–67]. In this study we asked how *L. monocytogenes* gains access to its basolateral receptors E-cadherin and c-Met in an intact epithelium since this bacterial pathogen is not known to actively disrupt the epithelial tight junctions.

We found that *L. monocytogenes* is able to invade a polarized epithelium from the apical side essentially only at vulnerable points formed by extrusion of senescent cells. As the first step of invasion, *L. monocytogenes* adhere almost exclusively over multicellular junctions, and adhesion is dependent on expression of InlA, suggesting that its receptor is available at these junctions. Indeed, when we pretreated the apical side of monolayers with an anti–E-cadherin blocking antibody, adhesion was significantly reduced, demonstrating that *L. monocytogenes* does access E-cadherin at junctional sites.

How does *L. monocytogenes* encounter E-cadherin across the tight junctions? It has been hypothesized that *L. monocytogenes* could breach the junctions though the activation of c-Met by InlB, since c-Met signaling modulates junction assembly [38,68]. However, we found that active disruption of the junctions was not necessary, since attachment occurs rapidly, since an *inlB*-mutant was not impaired for adhesion, and since E-cadherin is transiently exposed apically at normally occurring multicellular junction sites. Multicellular junctions represent only 2% of all junctions in a monolayer but are the sites of adhesion for 74% of all *L. monocytogenes*. Interestingly, invasion is even more specific for these sites than adhesion, since foci of intracellular *L. monocytogenes* are associated with multicellular junctions 97% of the time. These data compelled us to determine the nature of the multicellular junctions susceptible to *L. monocytogenes* invasion, identifying them as sites of apoptotic cell extrusion. During this process, senescent cells are released apically while the adjoining cells rapidly move in to seal the epithelial defect [46,47], forming a multicellular junction that persists for many hours.

Biochemical studies have shown that both tight junction proteins and adherens junction proteins are degraded in apoptotic cells, which may facilitate their detachment from neighboring cells [69–72]. Junctional remodeling creates a transient breach of the epithelial barrier, as it has been shown that cell extrusion produces localized defects in trans-epithelial electrical resistance [73]. We also documented junction remodeling and disruption, since the tight junctions at extrusion sites are reorganized basally in a funnel-like shape and since E-cadherin is exposed at these sites. These structural rearrangements render the multicellular junctions susceptible to apical invasion by *L. monocytogenes*. The sites of *L. monocytogenes* attachment to polarized monolayers are spatially closely associated with tight junctions, as marked by the scaffolding protein ZO-1. Previous work using freeze fracture and electron microscopy has shown that the tight junction strands surrounding extruding cells are in the process of being remodeled [74]. Several possibilities exist to explain the availability of E-cadherin to *L. monocytogenes* at these sites. For instance, tight junction strand remodeling could result in a local loss in fence function, and localization of E-cadherin above the tight junctions. Alternatively, the process of tight junction formation and remodeling may involve interactions between tight junction proteins, the scaffolding protein ZO-1, and the E-cadherin complex that could result in E-cadherin exposure on the apical surface [75].

The tropism of *L. monocytogenes* for extrusion sites is not exclusive to cultured cells but also occurs in vivo. Cell production within the intestinal crypts is balanced by cell shedding from the extrusion zone at the villus tips [51]. Therefore, we predicted this anatomical site would be the target for *L. monocytogenes* invasion in vivo. Studies exploring the initial site of *Listeria* entry in mice and rats have suggested that *L. monocytogenes* cannot invade enterocytes, but rather crosses the epithelium through M-cells of the Peyer's patches [26,28,76]. Although this may represent an important site of entry at very high inocula, it is unlikely to be the primary mode of epithelial invasion because mice and rats are not naturally susceptible to listeriosis due to differences in E-cadherin in the InlA binding region [13]. In contrast, an early electron microscopy study of intestinal tissue from orally inoculated guinea pigs found intracellular *L. monocytogenes* within enterocytes near the tips of the intestinal villi [30]. In another study using guinea pigs and transgenic mice expressing human E-cadherin in enterocytes, foci of *L. monocytogenes* were found within the intestinal villi near the apical tips [27]. Consistent with these observations, we found that *L. monocytogenes* adhere to and invade exclusively at the villus tips and found no bacteria invading lateral sides of villi, the intestinal crypts, or the Peyer's patches. Examining the villus tips more closely, we readily found that the invading bacteria were associated with multicellular junctions and the junctions surrounding protruding cells at the extrusion zone. Our results suggest that E-cadherin, and possibly other basolateral proteins, become exposed at the extrusion zone. We believe that cell extrusion sites will prove to be utilized by other pathogens as a general mechanism for accessing basolateral receptors.

Cell extrusion from the villus tips is a rapid and continuous process [51]. Therefore, in addition to providing a means for *L. monocytogenes* to evade the immune system [77], actin-based cell-to-cell spread within the villus tip may be beneficial to maintain an intracellular replicative niche in the face of a dynamically renewing system. The ability of *L. monocytogenes* to thrive and spread intracellularly is clearly responsible for its capacity to cause severe invasive disease and to disseminate to distant organs. However, *L. monocytogenes* causes invasive disease in immunocompetent individuals only rarely, after ingestion of very high numbers of bacteria [1], and instead is shed asymptomatically by at least 1% of healthy humans [78,79]. The mechanisms of asymptomatic carriage of *Listeria* have only recently come under investigation. One study in a murine model of infection found that *L. monocytogenes* survive extracellularly in the lumen of the gall bladder [80]. Since colonization of this anatomic site did not involve any of the known *L. monocytogenes* adaptations for intracellular survival, we speculate that an alternative mechanism of asymptomatic carriage may involve local invasion of the villus tips, intracellular replication, and cell-to-cell spread balanced by villus cell renewal.

Materials and Methods

MDCK cell culture. MDCK G/II cells were kindly provided by Dr. W. James Nelson (Stanford University, Stanford, California) and were

maintained at 37 °C in 5% CO_2 atmosphere in Gibco DMEM (Invitrogen, San Diego, California, United States) supplemented with 10% Gibco fetal bovine serum (Invitrogen). To culture polarized MDCK monolayers, cells were trypsinized and seeded on 12-mm polycarbonate tissue culture inserts (Transwell filters; Costar, Cambridge, Massachusetts, United States) at a density of 10^6 cells/cm^2 and supplemented with fresh basal media daily for 4 d. Verification of tight junction barrier function of intact monolayers was performed as described in [81] and shown in Figure S1. For apical versus basal comparison of *L. monocytogenes* infection, cells were cultured on 3-μm-pore Transwell filters. For all other experiments, cells were cultured on 0.4-μm-pore Transwell filters. To disrupt calcium-dependent intercellular junctions, immediately prior to infection, MDCK monolayers were incubated in low calcium media (5 μM Ca^{2+}; [81]) for 30 min, and then switched back to DMEM (1.8 mM Ca^{2+}).

***L. monocytogenes* strains and culture conditions.** 10403S, a Wt *L. monocytogenes* strain, and isogenic mutant strains DP-L4405 (Δ*inlA*), DP-L4406 (Δ*inlB*), and DP-L3078 (Δ*actA*) were kindly provided by Dr. Daniel A. Portnoy (University of California, Berkeley, California, United States) and have been described previously [45,82]. GFP-expressing 10403S strain DH-L1039 (Wt-GFP) was kindly provided by Dr. Darren E. Higgins (Harvard University, Boston, Massachusetts, United States) and has been described in [83,84]. JAT-395, 10403S that expresses monomeric red fluorescent protein fused to ActA (ActA-RFP) has recently been described [53]. *L. monocytogenes* were grown on Difco BHI-agar or in BHI-broth (BD Biosciences, San Jose, California). Cultures of ActA-RFP and Wt-GFP were supplemented with chloramphenicol. For infection, *L. monocytogenes* strains were inoculated with a loop from a fresh plate into 3-ml BHI-broth and grown 13–15 h at room temperature without agitation.

Assays of *L. monocytogenes* cell adherence and invasion. Bacterial cells were harvested at 10,000 g for 1 min and resuspended to 0.5 OD_{600} (7×10^8 CFU/ml) in room temperature DMEM. Immediately prior to infection, MDCK cells were transferred to 37 °C DMEM. *L. monocytogenes* were added to polarized MDCK cells at an MOI of 140:1 bacteria per cell in 500 μl of DMEM and were allowed to adhere for 10 min at 37 °C in 5% CO_2 atmosphere. Cell monolayers were washed by pipeting with 3 changes of fresh 37 °C DMEM to remove non-adhered *L. monocytogenes*. This point was considered time 0:00 for all analyses. Invasion of cells was allowed to proceed for 1 h in DMEM at 37 °C in 5% CO_2 atmosphere (1:00). The medium was replaced with DMEM containing 50 μg/ml gentamicin and incubated for 20 min to kill extracellular *L. monocytogenes* (1:20). Finally, the medium was replaced with DMEM containing 10 μg/ml gentamicin and incubated at 37 °C in 5% CO_2 atmosphere up to 5:00. At appropriate time points, the above infection sequence was interrupted in order to assay for *L. monocytogenes* adhesion, invasion, or intracellular replication as described below.

To assay for cell adhesion, at 0:00, monolayers were either fixed and analyzed by microscopy or dispersed and plated for colony forming units (CFUs). Adhesion by microscopic analysis was determined from at least three 40× fields (~2000 MDCK cells/field) from each of at least three infected monolayers per strain tested. For adhesion by CFU counts, the entire Transwell-monolayer excised from the frame was dispersed by 15 s of vortex agitation in 500 μl of phosphate-buffered saline (PBS) 1% saponin. Appropriate dilutions of the suspension were plated onto BHI-agar. Short-term PBS incubation and the presence of saponin were determined not to affect *L. monocytogenes* viability (unpublished data). To assay for cell invasion, at 1:20, monolayers were washed by pipeting with three changes of fresh 37 °C DMEM to remove gentamicin. Intracellular *L. monocytogenes* were recovered by 15 s of vortex agitation in 500 μl of PBS 1% saponin. Appropriate dilutions of the suspension were plated onto BHI-agar for CFU determination. For analysis of intracellular replication, at various time points, cell monolayers were fixed and analyzed by immunofluorescence microscopy. To determine the percentage of invasion sites at multicellular junctions, monolayers were fixed at 3:00. At least 100 randomly observed *L. monocytogenes* foci (or Δ*actA* infected cells) were analyzed from each of at least three infected monolayers for each strain tested. Experiments were performed at least three times. Prism software (GraphPad, San Diego, California, United States) was utilized for construction of graphs and statistical analysis of data. Student's *t*-test was used to compare two sample groups. ANOVA with Bonferroni post-tests were used to analyze three or more sample groups. Pearson product-moment correlation coefficient was used to analyze distributions.

Antibody blocking of *L. monocytogenes* cell adherence. E-cadherin was blocked with mouse mAb anti-E-cadherin antibody (rr1) [48,49], and gp135 was blocked with mouse mAb anti-gp135 (clone 3F2/DB) [50]. Both antibodies were kindly provided by Dr. W. James Nelson. To normalize the concentration of these antibodies, a dilution series of each was blotted under vacuum suction onto nitrocellulose using a 96-well biodot apparatus (Bio-Rad, Hercules, California, United States). The blot was allowed to dry fully, and then incubated for 1 h at room temperature in blocking solution containing a 1:1 mixture of Li-Cor blocking buffer (Li-Cor Biosciences, Lincoln, Nebraska) and PBS. The blot was incubated in goat anti-mouse Alexafluor660 antibodies (Molecular Probes, Eugene, Oregon, United States) diluted 1:5000 in blocking solution for 1 h. The blot was washed 3× for 5 min in PBS 0.1% Tween-20, 3× for 2 min in PBS, then imaged with a Li-Cor Odyssey infrared imaging system. The integrated fluorescence intensity for each dot was quantified using Li-Cor Odyssey software.

Polarized MDCK cells were blocked at 4 °C for 30 min in 100 μl of apically applied DMEM 10% FBS (Mock), gp135 antibody in undiluted hybridoma supernatant, or mouse monoclonal anti-E-cadherin antibody diluted in DMEM 10% FBS to the same effective concentration (equivalent dot-blot integrated fluorescence intensity) as the gp135 antibody. Cell monolayers were washed by pipeting with two changes of DMEM. *L. monocytogenes* were added to polarized MDCK cells at an MOI of 140:1 in 500 μl of media and were allowed to adhere for 5 min at room temperature. Cell monolayers were washed by pipeting with three changes of fresh room temperature DMEM to remove non-adhered *L. monocytogenes*. Cells and adherent *L. monocytogenes* were fixed and adhesion was quantified by microscopy analysis of at least three 40× fields from each of three infected monolayers per blocking condition.

***L. monocytogenes* infection of rabbit ileal loops.** The animal experimental protocol was reviewed and approved by the institutional animal care and use committee of Stanford University. Methods for ileal loop preparation and inoculation were modified from previous descriptions [41,85]. A New Zealand White rabbit weighing 2 kg was fasted for 36 h prior to surgery. After premedication with an intramuscular (IM) injection of glycopyrrolate (0.02 mg/kg), anesthesia was induced with ketamine (40 mg/kg IM) and xylazine (5 mg/kg IM). An intravenous catheter was placed to allow fluid administration during the surgery (20 ml/kg/hr lactated Ringer's solution), an endotracheal tube was placed, and anesthesia was maintained using isoflurane gas. A midline celiotomy was performed to expose the bowel. The ileocecal junction was identified, and the ileum was double ligated with silk ties just proximal to the sacculus rotundus. A series of ligated loops were then prepared starting with the terminal ileum and working retrograde along the small intestine with particular care taken to preserve the vasculature and keep the gut moist. Infected loops ranged in length from 4.5–5 cm in length. A non-inoculated "spacer" loop of 2–3 cm was left between all inoculated loops. Loops were stretched and measured after preparation and then inoculated with 4×10^7 CFU/ml of Wt-GFP or 4×10^8 CFU/ml Wt-GFP, Wt, Δ*inlA*, ActA-RFP *L. monocytogenes* in BHI broth using a 25-gauge needle to a volume of 0.1 ml per cm of loop to provide a uniform initial distention. After inoculation, the small intestine was returned to its normal anatomic position and the abdominal and skin incisions were sutured closed. Isoflurane administration was discontinued and the animal was moved to a recovery area and placed on a warm-water heating pad. The endotracheal tube was removed when the animal regained consciousness, and pain control was provided by the administration of hydromorphone post-operatively at a dose of 0.2 mg/kg IM, which was repeated every 2 h as needed. At the planned endpoint of 4 h post-inoculation, the animal was euthanized with an intravenous overdose of pentobarbital. Individual loops were harvested by incisions through spacer loops, and then opened, washed gently by dipping in sterile saline, and fixed flat (lumenal side up).

Microscopy and antibodies. Time-lapse microscopy was performed essentially as described in [86]. For immunofluorescence microscopy, samples were fixed with 2% paraformaldehyde in 100 mM phosphate buffer (pH 7.4) (15 min for cell monolayers, and 1 h for tissues), and were permeabilized in PBS 1% saponin 3% bovine serum albumin or left unpermeabilized by blocking samples and diluting antibodies/probes in PBS 3% BSA. After incubation with appropriate antibodies/probes, samples were mounted with Vectashield mounting medium (Vector Laboratories, Burlingame, California, United States) and imaged with a confocal microscope (Bio-Rad). For visualization of intestinal villi, we mounted intact tissue blocks and imaged the stained tissues without prior embedding and sectioning. The samples were imaged by confocal microscopy where optical sections were taken at 0.5-μm resolution through both the cell monolayers and the intestinal villi. Z-stacks were reconstructed into three dimensions using Volocity software (Improvision, Lexington, Massachusetts, United States). Figures were assembled with Photoshop software (Adobe, San Jose, California, United States).

L. monocytogenes were detected by incubation of samples with *Listeria* O antisera (rabbit) poly types 1 and 4, Difco, 1:600 dilution (BD Biosciences, San Jose, California, United States). Tight junctions were detected by incubating samples with mouse anti–ZO-1 antibodies (Zymed, South San Francisco, California, United States) at 1:300 dilution, and see [81]. E-cadherin was detected by incubating samples with mouse mAb rr1, an antibody that recognizes an extracellular epitope of E-cadherin at 1:50 to 1:100 dilution [48,49]. Gp135 was detected with mouse mAb anti-gp135 (clone 3F2/DB, undiluted hybridoma supernatant) [50]. Anti-IgG Alexa-fluor conjugated antibodies of appropriate species reactivity and fluorescence spectra were used for secondary detection (Molecular Probes). An immunofluorescence inside/outside staining that distinguishes extracellular from intracellular *L. monocytogenes* was modified from [87] with appropriate antibodies for this study. Actin was visualized by incubating samples with Alexa-fluor conjugated phalloidins (Molecular Probes). To visualize all nuclei, permeabilized samples were incubated with toto-3 (Molecular Probes). To visualize senescent cells, live samples were incubated with Sytox green (Molecular Probes).

Supporting Information

Figure S1. Preservation of Barrier Function during *L. monocytogenes* Infection of MDCK Cells Polarized on Transwell Filters

Triplicate samples of filters without cells, uninfected monolayers, and infected monolayers were examined. Confluent MDCK cells were polarized for 4 d on 0.4-μm Transwell filters prior to starting the experiments. At time zero, a set of monolayers was infected through the apical compartment, as described in Materials and Methods. After washing unattached bacteria, 500 ng of fluorescent dextran (conjugated to Alexa647 dye from Molecular Probes) diluted in media was added to the apical chambers. Samples from the basolateral compartment were collected at different timepoints, and the fluorescence intensity measured in a Li-Cor Odyssey scanner. A dilution series of dextran solution was used to generate a standard curve of fluorescence intensity relative to dextran concentration, and to determine the linear range of our measurements (top graph). A linear best-fit of the dilution series was used to calculate the background level (Y-intercept). The experimental samples were measured at 1 h intervals after start of infection. The fluorescence intensity was background subtracted, converted to a dextran quantity. Negative values were normalized to zero. The amount of dextran found in the basolateral compartment was plotted over time (bottom graph). Error bars represent one standard deviation from the mean of three independent samples.

Found at DOI: 10.1371/journal.ppat.0020003.sg001 (42 KB PDF).

Figure S2. Increased E-cadherin Exposure and *L. monocytogenes* Adhesion in Calcium-Depleted MDCK Monolayers

Polarized MDCK monolayers were untreated (Control) or incubated in low calcium medium (Low Ca^{2+}) prior to apical infection with Wt *L. monocytogenes* at an MOI of 140:1 for 10 min.
(A) Adhesion was determined by dispersion and plating for CFUs. Means and standard deviations of CFU/1,000 cells from triplicate samples are shown. Sample groups are significantly different: unpaired *t*-test $p < 0.001$.
(B) Region of a low Ca^{2+} monolayer stained for *L. monocytogenes* (green) and ZO-1 (red).
(C) Region of a low Ca^{2+} monolayer left unpermeabilized and stained for *L. monocytogenes* (green) and E-cadherin (red).
Scale bars 10 μm.

Found at DOI: 10.1371/journal.ppat.0020003.sg002 (466 KB JPG).

Figure S3. Lack of Association of *L. monocytogenes* Invasion with the Intestinal Crypts or the Peyer's Patches; *inlA*-mutant Is Noninvasive

(A) A rabbit ileal loop was infected with 4×10^7 CFU/ml of Wt *L. monocytogenes* expressing GFP (Wt-GFP) for 4 h. Optical sections through crypt-villus axis did not reveal *L. monocytogenes* associated with the intestinal crypts (arrows). *L. monocytogenes* were found at the tips of the villi (inset). Tissue was stained with antibodies to ZO-1 (red) and with toto-3 for nuclei (blue).
(B) A rabbit ileal loop with a Peyer's patch was infected with 4×10^8 CFU/ml of Wt-GFP *L. monocytogenes* for 4 h. Tissue was stained with phalloidin for F-actin (red). *L. monocytogenes* were not found associated with the follicle associated epithelium overlying the Peyer's patch, (C) but were found at the tips of adjacent villi.
(D) A rabbit ileal loop was infected with 4×10^8 CFU/ml of ActA-RFP *L. monocytogenes* for 4 h. Red fluorescent bacteria were only found within cells at the tips of the villi stained with phalloidin for F-actin (blue).
(E) A rabbit ileal loop was infected with 4×10^8 CFU/ml of Δ*inlA L. monocytogenes* for 4 h. Tissue was stained with antibodies to *L. monocytogenes* (green), with fluorescent phalloidin for F-actin (red) and with toto-3 for nuclei. Optical section through a three-dimensional reconstruction of villus tips is shown. No intracellular Δ*inlA L. monocytogenes* were found.

Found at DOI: 10.1371/journal.ppat.0020003.sg003 (1.7 MB JPG).

Video S1. Cell Extrusion

QuickTime DIC time-lapse video of cell extrusion from MDCK monolayer, shown in Figure 4A. Viewing requires QuickTime (free download from: http://www.apple.com/quicktime/download).

Found at DOI: 10.1371/journal.ppat.0020003.sv001 (555 KB MOV).

Video S2. *L. monocytogenes* Adhesion at Site of Cell Extrusion

QuickTime Virtual Reality video of Figure 5A.

Found at DOI: 10.1371/journal.ppat.0020003.sv002 (7.1 MB MOV).

Video S3. Villus Tip Infected with Wt *L. monocytogenes*

QuickTime movie of a complete optical scan through a rabbit intestinal villus tip infected with Wt-GFP *L. monocytogenes* (green), and counterstained with phalloidin (red) to visualize the cytoskeleton, and with toto-3 (blue) to visualize nuclei.

Found at DOI: 10.1371/journal.ppat.0020003.sv003 (574 KB MOV).

Video S4. Villus Tip Infected with Δ*inlA L. monocytogenes*

QuickTime movie of an intestinal villus tip processed as in Video S3, but infected with 10× the amount (4×10^8 CFU/ml) of Δ*inlA L. monocytogenes* (green) than shown for Wt-GFP *L. monocytogenes*. Cells were counterstained with phalloidin (red) to visualize the cytoskeleton and toto-3 (blue) to visualize nuclei.

Found at DOI: 10.1371/journal.ppat.0020003.sv004 (417 KB MOV).

Acknowledgments

We are indebted to Roger Vogelmann, Susanne Rafelski, Alex Nielsen, Denise Monack, Stanley Falkow, W. James Nelson, Michael Howitt, and Fabio Bagnoli for technical assistance, experimental suggestions, and helpful discussions, and to Daniel A. Portnoy and Darren E. Higgins for providing bacterial strains. We thank Stanley Falkow, Denise Monack, and Roger Vogelmann for comments on the manuscript. A Cell and Molecular Biology Training Grant from the National Institutes of Health (5 T32 GM07276) supported MP. This work was supported by a grant from the National Institutes of Health (RO1-AI36929) awarded to JAT, and grants PO3 DK56339 and MedImmune Career Development Award to MRA.

Author contributions. MP, GO, JAT, and MRA conceived and designed the experiments. MP, GO, and MRA performed the experiments. MP, JAT, and MRA analyzed the data and wrote the manuscript. JAT and MRA contributed equally as senior authors.

Competing interests. The authors have declared that no competing interests exist. ■

References

1. Vazquez-Boland JA, Kuhn M, Berche P, Chakraborty T, Dominguez-Bernal G, et al. (2001) Listeria pathogenesis and molecular virulence determinants. Clin Microbiol Rev 14: 584–640.
2. Mead PS, Slutsker L, Dietz V, McCaig LF, Bresee JS, et al. (1999) Food-related illness and death in the United States. Emerg Infect Dis 5: 607–625.
3. Murray EDG, Webb RA, Swann MBR (1926) A disease of rabbits characterized by a large mononuclear leukocytosis, caused by a hitherto undescribed bacillus *Bacterium monocytogenes* (n. sp.). J Pathol Bacteriol 29: 407–439.
4. Pinner RW, Schuchat A, Swaminathan B, Hayes PS, Deaver KA, et al. (1992) Role of foods in sporadic listeriosis. II. Microbiologic and epidemiologic investigation. The Listeria Study Group. JAMA 267: 2046–2050.
5. Farber JM, Peterkin PI (1991) *Listeria monocytogenes*, a food-borne pathogen. Microbiol Rev 55: 476–511.
6. Gaillard JL, Berche P, Frehel C, Gouin E, Cossart P (1991) Entry of *L. monocytogenes* into cells is mediated by internalin, a repeat protein

reminiscent of surface antigens from gram-positive cocci. Cell 65: 1127–1141.
7. Cabanes D, Dehoux P, Dussurget O, Frangeul L, Cossart P (2002) Surface proteins and the pathogenic potential of *Listeria monocytogenes*. Trends Microbiol 10: 238–245.
8. Dramsi S, Biswas I, Maguin E, Braun L, Mastroeni P, et al. (1995) Entry of *Listeria monocytogenes* into hepatocytes requires expression of inIB, a surface protein of the internalin multigene family. Mol Microbiol 16: 251–261.
9. Mengaud J, Ohayon H, Gounon P, Mege RM, Cossart P (1996) E-cadherin is the receptor for internalin, a surface protein required for entry of *L. monocytogenes* into epithelial cells. Cell 84: 923–932.
10. da Silva Tatley F, Aldwell FE, Dunbier AK, Guilford PJ (2003) N-terminal E-cadherin peptides act as decoy receptors for *Listeria monocytogenes*. Infect Immun 71: 1580–1583.
11. Lecuit M, Ohayon H, Braun L, Mengaud J, Cossart P (1997) Internalin of *Listeria monocytogenes* with an intact leucine-rich repeat region is sufficient to promote internalization. Infect Immun 65: 5309–5319.
12. Schubert WD, Urbanke C, Ziehm T, Beier V, Machner MP, et al. (2002) Structure of internalin, a major invasion protein of *Listeria monocytogenes*, in complex with its human receptor E-cadherin. Cell 111: 825–836.
13. Lecuit M, Dramsi S, Gottardi C, Fedor-Chaiken M, Gumbiner B, et al. (1999) A single amino acid in E-cadherin responsible for host specificity towards the human pathogen *Listeria monocytogenes*. EMBO J 18: 3956–3963.
14. Shen Y, Naujokas M, Park M, Ireton K (2000) InIB-dependent internalization of Listeria is mediated by the Met receptor tyrosine kinase. Cell 103: 501–510.
15. Li N, Xiang GS, Dokainish H, Ireton K, Elferink LA (2005) The listeria protein internalin B mimics hepatocyte growth factor-induced receptor trafficking. Traffic 6: 459–473.
16. Greiffenberg L, Goebel W, Kim KS, Weiglein I, Bubert A, et al. (1998) Interaction of *Listeria monocytogenes* with human brain microvascular endothelial cells: InlB-dependent invasion, long-term intracellular growth, and spread from macrophages to endothelial cells. Infect Immun 66: 5260–5267.
17. Lingnau A, Domann E, Hudel M, Bock M, Nichterlein T, et al. (1995) Expression of the *Listeria monocytogenes* EGD inlA and inlB genes, whose products mediate bacterial entry into tissue culture cell lines, by PrfA-dependent and -independent mechanisms. Infect Immun 63: 3896–3903.
18. Parida SK, Domann E, Rohde M, Muller S, Darji A, et al. (1998) Internalin B is essential for adhesion and mediates the invasion of *Listeria monocytogenes* into human endothelial cells. Mol Microbiol 28: 81–93.
19. Banerjee M, Copp J, Vuga D, Marino M, Chapman T, et al. (2004) GW domains of the *Listeria monocytogenes* invasion protein InlB are required for potentiation of Met activation. Mol Microbiol 52: 257–271.
20. Marino M, Banerjee M, Jonquieres R, Cossart P, Ghosh P (2002) GW domains of the *Listeria monocytogenes* invasion protein InlB are SH3-like and mediate binding to host ligands. EMBO J 21: 5623–5634.
21. Copp J, Marino M, Banerjee M, Ghosh P, van der Geer P (2003) Multiple regions of internalin B contribute to its ability to turn on the Ras-mitogen-activated protein kinase pathway. J Biol Chem 278: 7783–7789.
22. Marino M, Braun L, Cossart P, Ghosh P (1999) Structure of the lnlB leucine-rich repeats, a domain that triggers host cell invasion by the bacterial pathogen *L. monocytogenes*. Mol Cell 4: 1063–1072.
23. Ireton K, Payrastre B, Cossart P (1999) The *Listeria monocytogenes* protein InlB is an agonist of mammalian phosphoinositide 3-kinase. J Biol Chem 274: 17025–17032.
24. Bergmann B, Raffelsbauer D, Kuhn M, Goetz M, Hom S, et al. (2002) InlA- but not InlB-mediated internalization of *Listeria monocytogenes* by non-phagocytic mammalian cells needs the support of other internalins. Mol Microbiol 43: 557–570.
25. MacDonald TT, Carter PB (1980) Cell-mediated immunity to intestinal infection. Infect Immun 28: 516–523.
26. Marco AJ, Prats N, Ramos JA, Briones V, Blanco M, et al. (1992) A microbiological, histopathological and immunohistological study of the intragastric inoculation of *Listeria monocytogenes* in mice. J Comp Pathol 107: 1–9.
27. Lecuit M, Vandormael-Pournin S, Lefort J, Huerre M, Gounon P, et al. (2001) A transgenic model for listeriosis: Role of internalin in crossing the intestinal barrier. Science 292: 1722–1725.
28. Jensen VB, Harty JT, Jones BD (1998) Interactions of the invasive pathogens Salmonella typhimurium, *Listeria monocytogenes*, and Shigella flexneri with M cells and murine Peyer's patches. Infect Immun 66: 3758–3766.
29. Pron B, Boumaila C, Jaubert F, Sarnacki S, Monnet JP, et al. (1998) Comprehensive study of the intestinal stage of listeriosis in a rat ligated ileal loop system. Infect Immun 66: 747–755.
30. Racz P, Tenner K, Mero E (1972) Experimental Listeria enteritis. I. An electron microscopic study of the epithelial phase in experimental listeria infection. Lab Invest 26: 694–700.
31. Boller K, Vestweber D, Kemler R (1985) Cell-adhesion molecule uvomorulin is localized in the intermediate junctions of adult intestinal epithelial cells. J Cell Biol 100: 327–332.
32. Boyle EC, Finlay BB (2003) Bacterial pathogenesis: Exploiting cellular adherence. Curr Opin Cell Biol 15: 633–639.
33. Sousa S, Lecuit M, Cossart P (2005) Microbial strategies to target, cross or disrupt epithelia. Curr Opin Cell Biol 17: 489–498.
34. Gaillard JL, Finlay BB (1996) Effect of cell polarization and differentiation on entry of *Listeria monocytogenes* into the enterocyte-like Caco-2 cell line. Infect Immun 64: 1299–1308.
35. Temm-Grove CJ, Jockusch BM, Rohde M, Niebuhr K, Chakraborty T, et al. (1994) Exploitation of microfilament proteins by *Listeria monocytogenes*: Microvillus-like composition of the comet tails and vectorial spreading in polarized epithelial sheets. J Cell Sci 107 (Pt 10): 2951–2960.
36. Cossart P, Pizarro-Cerda J, Lecuit M (2003) Invasion of mammalian cells by *Listeria monocytogenes*: Functional mimicry to subvert cellular functions. Trends Cell Biol 13: 23–31.
37. Crepaldi T, Pollack AL, Prat M, Zborek A, Mostov K, et al. (1994) Targeting of the SF/HGF receptor to the basolateral domain of polarized epithelial cells. J Cell Biol 125: 313–320.
38. Balkovetz DF, Pollack AL, Mostov KE (1997) Hepatocyte growth factor alters the polarity of Madin-Darby canine kidney cell monolayers. J Biol Chem 272: 3471–3477.
39. Nelson WJ (2003) Adaptation of core mechanisms to generate cell polarity. Nature 422: 766–774.
40. Robbins JR, Barth AI, Marquis H, de Hostos EL, Nelson WJ, et al. (1999) *Listeria monocytogenes* exploits normal host cell processes to spread from cell to cell. J Cell Biol 146: 1333–1350.
41. Burrows W, Musteikis GM (1966) Cholera infection and toxin in the rabbit ileal loop. J Infect Dis 116: 183–190.
42. Tilney LG, Portnoy DA (1989) Actin filaments and the growth, movement, and spread of the intracellular bacterial parasite, *Listeria monocytogenes*. J Cell Biol 109: 1597–1608.
43. Kocks C, Gouin E, Tabouret M, Berche P, Ohayon H, et al. (1992) *L. monocytogenes*–induced actin assembly requires the actA gene product, a surface protein. Cell 68: 521–531.
44. Domann E, Wehland J, Rohde M, Pistor S, Hartl M, et al. (1992) A novel bacterial virulence gene in *Listeria monocytogenes* required for host cell microfilament interaction with homology to the proline-rich region of vinculin. EMBO J 11: 1981–1990.
45. Skoble J, Portnoy DA, Welch MD (2000) Three regions within ActA promote Arp2/3 complex-mediated actin nucleation and *Listeria monocytogenes* motility. J Cell Biol 150: 527–538.
46. Corfe BM, Dive C, Garrod DR (2000) Changes in intercellular junctions during apoptosis precede nuclear condensation or phosphatidylserine exposure on the cell surface. Cell Death Differ 7: 234–235.
47. Rosenblatt J, Raff MC, Cramer LP (2001) An epithelial cell destined for apoptosis signals its neighbors to extrude it by an actin- and myosin-dependent mechanism. Curr Biol 11: 1847–1857.
48. Gumbiner B, Simons K (1986) A functional assay for proteins involved in establishing an epithelial occluding barrier: Identification of a uvomorulin-like polypeptide. J Cell Biol 102: 457–468.
49. Gumbiner B, Simons K (1987) The role of uvomorulin in the formation of epithelial occluding junctions. Ciba Found Symp 125: 168–186.
50. Ojakian GK, Schwimmer R (1988) The polarized distribution of an apical cell surface glycoprotein is maintained by interactions with the cytoskeleton of Madin-Darby canine kidney cells. J Cell Biol 107: 2377–2387.
51. Babyatsky MW, Podolsky DK (2003) Growth and Development of the Gastrointestinal Tract. In: Yamada T, editor. Textbook of gastroenterology. Philadelphia: Lippincott Williams & Wilkins. pp. 521–556.
52. Sancho E, Batlle E, Clevers H (2004) Signaling pathways in intestinal development and cancer. Annu Rev Cell Dev Biol 20: 695–723.
53. Rafelski SM, Theriot JA (2005) Bacterial shape and ActA distribution affect initiation of *Listeria monocytogenes* actin-based motility. Biophys J 89: 2146–2158.
54. Freitag NE, Jacobs KE (1999) Examination of *Listeria monocytogenes* intracellular gene expression by using the green fluorescent protein of Aequorea victoria. Infect Immun 67: 1844–1852.
55. Shetron-Rama LM, Marquis H, Bouwer HG, Freitag NE (2002) Intracellular induction of *Listeria monocytogenes* actA expression. Infect Immun 70: 1087–1096.
56. Vogelmann R, Amieva MR, Falkow S, Nelson WJ (2004) Breaking into the epithelial apical-junctional complex—News from pathogen hackers. Curr Opin Cell Biol 16: 86–93.
57. Barragan A, Brossier F, Sibley LD (2005) Transepithelial migration of *Toxoplasma gondii* involves an interaction of intercellular adhesion molecule 1 (ICAM-1) with the parasite adhesin MIC2. Cell Microbiol 7: 561–568.
58. Guerrero CA, Mendez E, Zarate S, Isa P, Lopez S, et al. (2000) Integrin alpha(v)beta(3) mediates rotavirus cell entry. Proc Natl Acad Sci U S A 97: 14644–14649.
59. Mounier J, Vasselon T, Hellio R, Lesourd M, Sansonetti PJ (1992) Shigella flexneri enters human colonic Caco-2 epithelial cells through the basolateral pole. Infect Immun 60: 237–248.
60. Wu Z, Nybom P, Magnusson KE (2000) Distinct effects of *Vibrio cholerae* haemagglutinin/protease on the structure and localization of the tight junction-associated proteins occludin and ZO-1. Cell Microbiol 2: 11–17.
61. Amieva MR, Vogelmann R, Covacci A, Tompkins LS, Nelson WJ, et al. (2003) Disruption of the epithelial apical-junctional complex by *Helicobacter pylori* CagA. Science 300: 1430–1434.
62. Dean P, Kenny B (2004) Intestinal barrier dysfunction by enteropathogenic *Escherichia coli* is mediated by two effector molecules and a bacterial surface protein. Mol Microbiol 54: 665–675.
63. Isberg RR, Leong JM (1990) Multiple beta 1 chain integrins are receptors

for invasin, a protein that promotes bacterial penetration into mammalian cells. Cell 60: 861–871.
64. Isberg RR, Voorhis DL, Falkow S (1987) Identification of invasin: A protein that allows enteric bacteria to penetrate cultured mammalian cells. Cell 50: 769–778.
65. Autenrieth IB, Firsching R (1996) Penetration of M cells and destruction of Peyer's patches by *Yersinia enterocolitica*: An ultrastructural and histological study. J Med Microbiol 44: 285–294.
66. Clark MA, Hirst BH, Jepson MA (1998) M-cell surface beta1 integrin expression and invasin-mediated targeting of Yersinia pseudotuberculosis to mouse Peyer's patch M cells. Infect Immun 66: 1237–1243.
67. Marra A, Isberg RR (1997) Invasin-dependent and invasin-independent pathways for translocation of *Yersinia pseudotuberculosis* across the Peyer's patch intestinal epithelium. Infect Immun 65: 3412–3421.
68. Grisendi S, Arpin M, Crepaldi T (1998) Effect of hepatocyte growth factor on assembly of zonula occludens-1 protein at the plasma membrane. J Cell Physiol 176: 465–471.
69. Bojarski C, Weiske J, Schoneberg T, Schroder W, Mankertz J, et al. (2004) The specific fates of tight junction proteins in apoptotic epithelial cells. J Cell Sci 117: 2097–2107.
70. Schmeiser K, Grand RJ (1999) The fate of E- and P-cadherin during the early stages of apoptosis. Cell Death Differ 6: 377–386.
71. Steinhusen U, Weiske J, Badock V, Tauber R, Bommert K, et al. (2001) Cleavage and shedding of E-cadherin after induction of apoptosis. J Biol Chem 276: 4972–4980.
72. Keller SH, Nigam SK (2003) Biochemical processing of E-cadherin under cellular stress. Biochem Biophys Res Commun 307: 215–223.
73. Gitter AH, Bendfeldt K, Schulzke JD, Fromm M (2000) Leaks in the epithelial barrier caused by spontaneous and TNF-alpha-induced single-cell apoptosis. FASEB J 14: 1749–1753.
74. Madara JL (1990) Maintenance of the macromolecular barrier at cell extrusion sites in intestinal epithelium: Physiological rearrangement of tight junctions. J Membr Biol 116: 177–184.
75. Rajasekaran AK, Hojo M, Huima T, Rodriguez-Boulan E (1996) Catenins and zonula occludens-1 form a complex during early stages in the assembly of tight junctions. J Cell Biol 132: 451–463.
76. Marco AJ, Altimira J, Prats N, Lopez S, Dominguez L, et al. (1997) Penetration of *Listeria monocytogenes* in mice infected by the oral route. Microb Pathog 23: 255–263.
77. Portnoy DA, Auerbuch V, Glomski IJ (2002) The cell biology of *Listeria monocytogenes* infection: The intersection of bacterial pathogenesis and cell-mediated immunity. J Cell Biol 158: 409–414.
78. Bojsen-Moller J (1972) Human listeriosis. Diagnostic, epidemiological and clinical studies. Acta Pathol Microbiol Scand [B] Microbiol Immunol (Suppl) 229: 1–157.
79. Muller HE (1990) Listeria isolations from feces of patients with diarrhea and from healthy food handlers. Infection 18: 97–99.
80. Hardy J, Francis KP, DeBoer M, Chu P, Gibbs K, et al. (2004) Extracellular replication of *Listeria monocytogenes* in the murine gall bladder. Science 303: 851–853.
81. Vogelmann R, Nelson WJ (2005) Fractionation of the epithelial apical junctional complex: Reassessment of protein distributions in different substructures. Mol Biol Cell 16: 701–716.
82. Bakardjiev AI, Stacy BA, Fisher SJ, Portnoy DA (2004) Listeriosis in the pregnant guinea pig: A model of vertical transmission. Infect Immun 72: 489–497.
83. Shen A, Higgins DE (2005) The 5′ untranslated region-mediated enhancement of intracellular listeriolysin O production is required for *Listeria monocytogenes* pathogenicity. Mol Microbiol 57: 1460–1473.
84. Agaisse H, Burrack LS, Philips JA, Rubin EJ, Perrimon N, et al. (2005) Genome-wide RNAi screen for host factors required for intracellular bacterial infection. Science 309: 1248–1251.
85. De SN, Chatterje DN (1953) An experimental study of the mechanism of action of *Vibrio cholerae* on the intestinal mucous membrane. J Pathol Bacteriol 66: 559–562.
86. Bagnoli F, Buti L, Tompkins L, Covacci A, Amieva MR (2005) *Helicobacter pylori* CagA induces a transition from polarized to invasive phenotypes in MDCK cells. Proc Natl Acad Sci U S A 102: 16339–16344.
87. Amieva MR, Salama NR, Tompkins LS, Falkow S (2002) *Helicobacter pylori* enter and survive within multivesicular vacuoles of epithelial cells. Cell Microbiol 4: 677–690.